Formation of Hollow Nanocrystals Through the Nanoscale Kirkendall Effect

Yadong Yin, Robert M. Rioux, Can K. Erdonmez, Steven Hughes, Gabor A. Somorjai, A. Paul Alivisatos*

Hollow nanocrystals can be synthesized through a mechanism analogous to the Kirkendall Effect, in which pores form because of the difference in diffusion rates between two components in a diffusion couple. Starting with cobalt nanocrystals, we show that their reaction in solution with oxygen and either sulfur or selenium leads to the formation of hollow nanocrystals of the resulting oxide and chalcogenides. This process provides a general route to the synthesis of hollow nanostructures of a large number of compounds. A simple extension of the process yielded platinum–cobalt oxide yolk-shell nanostructures, which may serve as nanoscale reactors in catalytic applications.

Porous solid materials are important in many areas of modern science and technology, including ion exchange, molecular separation, catalysis, chromatography, microelectronics, and energy storage (*1*–*3*). Notable examples are microporous (<2-nm) zeolites and mesoporous (2- to 50-nm) silicate and carbonaceous materials. The ability to manipulate the structure and morphology of porous solids on a nanometer scale would enable greater control of the local chemical environment (*4*–*6*). We demonstrate that nanoscale pores can develop inside nanocrystals with a mechanism analogous to void formation in the Kirkendall Effect, in which the mutual diffusion rates of two components in a diffusion couple differ by a considerable amount (*7*). We choose cobalt nanocrystals as a starting material to show that hollow nanocrystals of cobalt oxide and chalcogenides can be successfully synthesized through the reaction of cobalt colloidal solution with oxygen and either sulfur or selenium.

It has been known for more than half a century that porosity may result from differential solid-state diffusion rates of the reactants in an alloying or oxidation reaction. In 1947, Smigelkas and Kirkendall reported the movement of the interface between a diffusion couple, i.e., copper and zinc in brass, as the result of the different diffusion rates of these two species at an elevated temperature (*7*). This phenomenon, now called the Kirkendall Effect, was the first experimental proof that atomic diffusion occurs through vacancy exchange and not by the direct interchange of atoms. The net directional flow of matter is balanced by an opposite flow of vacancies, which can condense into pores or annihilate at dislocations. Directional material flows also result from coupled reaction-diffusion phenomena at solid/gas or solid/liquid interfaces, leading to deformation, void formation, or both during the growth of metal oxide or sulfide films (*8*, *9*). These voids are usually explained by outward transport of fast-moving cations through the oxide layer and a balancing inward flow of vacancies to the vicinity of the metal-oxide interface. Interface motion and the formation of pores have been studied because of their impact on the reproducibility and reliability of solders, passivation layers, diffusion barriers, etc., but not generally as a method of preparing porous materials. The pores produced at a metal-metal diffusion couple or near the metal-oxide interface of a growing oxide do not yield monodisperse, ordered arrays but instead form a very heterogeneous ensemble. The observed volume fraction for pores is also commonly much smaller than would be expected for the known material flows. These observations are a direct result of the large volume of material that vacancies can diffuse into and the large number of defects with which they can react (*10*).

If the faster-diffusing species is confined into a nanocrystal core, the net rate of vacancy injection should increase markedly, because of the high surface-to-volume ratio of the particle and the absence of defects in the core. Within the small volume of a transforming nanocrystal, the supersaturated vacancy cloud is likely to coalesce into a single void. Previous studies on the interdiffusion of 30-μm powders with layered composition showed a large volume fraction of pores, but the geometry and distribution of the pores were not uniform, probably because of aggregation and the bulk-like dimension of the particles (*11*). Considerable progress has recently been made in synthesizing colloidal nanocrystals with well-controlled size, shape, and surface properties (*12*–*14*). Employing such high-quality nanocrystals as the starting materials, it should be possible to produce a relatively uniform population of hollow nanostructures.

We chose cobalt nanocrystals as the main starting material. A number of chemical methods have been developed to synthesize uniform cobalt nanocrystals in solution (*12*, *15*). Furthermore, cobalt reacts readily with other species such as sulfur and oxygen. Because cobalt is the major component in one class of superalloys, its high-temperature oxidation and sulfidation have been well studied (*16*, *17*). It is known that oxidation and sulfidation of bulk cobalt under vapor at high temperature are mainly controlled by outward diffusion of cobalt cations (*18*). This mode of growth operating on nanocrystals is expected to lead to hollow structures.

Sulfidation of cobalt was the first case in which we observed hollow nanostructures. Cobalt sulfide hollow nanospheres were synthesized in one pot by immediate injection of a solution of sulfur in *o*-dichlorobenzene into a hot cobalt nanocrystal dispersion (Fig. 1A) that was prepared by literature methods (*15*, *19*). At 455 K, the reaction between cobalt and sulfur completes within a few seconds, resulting in a black solution of cobalt sulfide nanocrystals. We confirmed that hollow particles are produced at temperatures as low as 373 K. The hollow particles are very stable in solution, suggesting that the chemical transformation of the surface did not disrupt the coating of the nanocrystals by surfactant molecules. When washed with methanol, the surfactant layer was removed, and it was no longer possible to redissolve the precipitate in *o*-dichlorobenzene.

Outward flow of cobalt through the sulfide shell resulted in supersaturation of vacancies, which condensed to form a single hole in each nanoparticle (Fig. 1, B and D). Two stable cobalt sulfide phases were observed, linnaeite (Co_3S_4) and cobalt pentlandite (Co_9S_8), depending on the sulfur-to-cobalt molar ratio used in the synthesis. X-ray powder diffraction (XRD) patterns in Fig. 1E show the evolution of the crystal structure as the molar ratio of sulfur to cobalt was increased. Co_9S_8 was the only sulfide phase observed when the molar ratio was lower than 9:8, whereas Co_3S_4 also appeared in the patterns when the molar ratio slightly exceeded this value. Only Co_3S_4 was obtained when the molar ratio of sulfur to cobalt was above 3:4. The size distribution of the sulfide hollow particles was similar to that of the starting cobalt nanocrystals. Monodisperse, hollow nanocrystals self-assembled into ordered hexagonal arrangements when evaporated slowly on the surface of a carbon-coated transmission electron microscopy (TEM) grid. The

Department of Chemistry, University of California at Berkeley, and Materials Science Division, Lawrence Berkeley National Laboratory, Berkeley, CA 94720, USA.

*To whom correspondence should be addressed. E-mail: alivis@uclink4.berkeley.edu

assembly process was driven by surface tension and van der Waals forces. Cobalt sulfide nanocrystals did not form superlattices as readily as cobalt nanocrystals do, probably because of a diminished van der Waals force (*19*). Assemblies of hollow nanoparticles present a distinct topology of ordered porous materials. In terms of the accessibility of pores from the outside, they fall between mesoporous materials with accessible channels and void lattices in which pores are confined in a continuous matrix (*20*).

Kinematical diffraction simulations (fig. S1) indicated that the XRD peaks are too broad to be consistent with a single crystal shell of the dimensions observed by TEM (*21*). We obtained satisfactory fits to the data in Fig. 1E, panels (d) and (g), by assuming ~4-nm, cubic crystalline domains. The fits also provided a confirmation of our phase assignments. TEM micrographs (Fig. 1D) of the same sample show that the average outer diameter of the hollow Co_9S_8 nanocrystals is ~15 nm. A reasonable explanation is that the shell of each hollow sphere is multicrystalline. This was confirmed by high-resolution TEM (HRTEM), which shows that both Co_9S_8 and Co_3S_4 hollow nanocrystals are composed of multiple crystallographic domains (Fig. 1C). The arrangement of the domains is analogous to the columnar morphology of grains often observed in thin film growth. The multicrystalline structure implies possible applications of these hollow nanocrystals as nanoscale reactors, because small molecules may be able to penetrate the shell through the grain boundaries.

In all instances of sulfidation, we found that the diameter of the hole in the center of the nanocrystals was 40 to 70% of the initial particle size (starting with cobalt particles with a size distribution of 7%, a single synthesis yielded a hole-size distribution of 13%). If sulfur transport through the growing shell were negligible, as shown for bulk sulfidation by marker experiments (*18*), then the two diameters would be expected to be identical. Significant inward sulfur transport could occur through grain boundaries or during the formation of the first few monolayers of sulfide. It is also possible that inward relaxation of the hole occurs, due to annihilation of vacancies at a semicoherent or incoherent cobalt-sulfide interface. Finally, the estimation of the hole size by visual inspection of TEM images may produce systematic errors. We attempted to examine the possibility of inward sulfur transport by performing the Co_3S_4 synthesis at different sulfur concentrations. Increased sulfur concentration increased hole size and enhanced outward growth of the shell, indicating that cobalt mobility rather than sulfur mobility was affected. This finding is consistent with bulk sulfidation studies (*18*), in which it is observed that an increased sulfur vapor pressure leads to injection of more cation vacancies into the growing sulfide and enhances the parabolic rate constant for sulfide growth.

For bulk cobalt, the rates of oxidation are 3 to 4 orders of magnitude lower than those of sulfidation above 750 K (*18*). This is also true under the conditions we used to produce hollow nanocrystals, and oxidation of nanocrystals took ~3 hours at 455 K. Figure 2, A to D, shows the evolution of the morphology of the nanocrystals with time as an O_2/Ar mixture is flowed through the cobalt colloidal solution. The XRD shows the presence of metallic cobalt up to 30 min after the start of the O_2/Ar flow (Fig. 2E). The solution of particles still displayed weak ferrofluidic response to a 1-T magnet

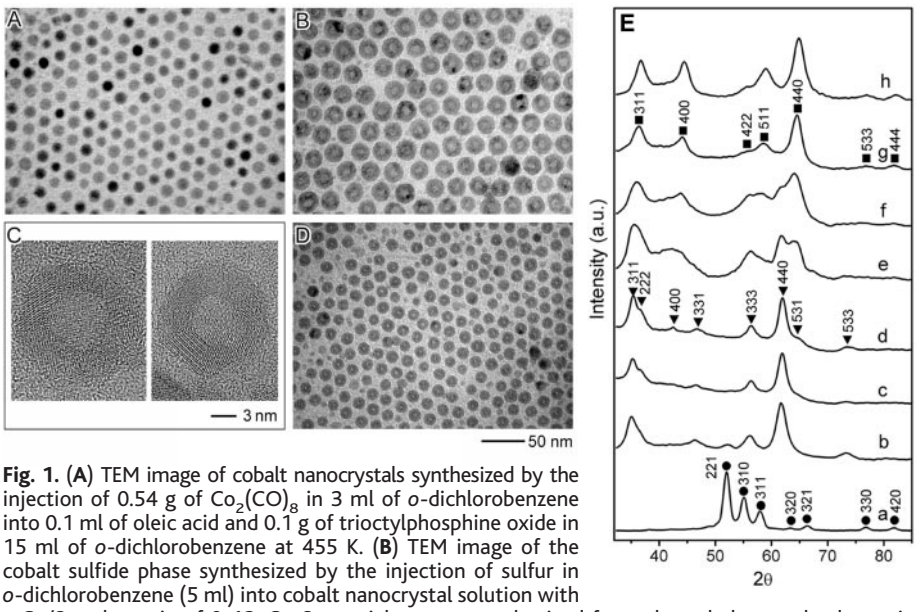

Fig. 1. (**A**) TEM image of cobalt nanocrystals synthesized by the injection of 0.54 g of $Co_2(CO)_8$ in 3 ml of *o*-dichlorobenzene into 0.1 ml of oleic acid and 0.1 g of trioctylphosphine oxide in 15 ml of *o*-dichlorobenzene at 455 K. (**B**) TEM image of the cobalt sulfide phase synthesized by the injection of sulfur in *o*-dichlorobenzene (5 ml) into cobalt nanocrystal solution with a Co/S molar ratio of 9:12. Co_3S_4 particles were synthesized from the cobalt sample shown in (A). (**C**) HRTEM images of Co_3S_4 (left) and Co_9S_8 (right). (**D**) TEM image of the cobalt sulfide phase synthesized as in (B), but with a Co:S molar ratio of 9:8. Co_9S_8 particles started from another cobalt sample that had an average diameter of ~11 nm. (**E**) XRD patterns of (a) cobalt nanocrystals and (b to h) cobalt sulfide synthesized with different Co/S molar ratios: (b) 9:5, (c) 9:7, (d) 9:8, (e) 9:10, (f) 9:11, (g) 9:12, and (h) 9:18. The dots, triangles, and squares represent peaks from cobalt, CO_9S_8, and CO_3S_4 phases, respectively.

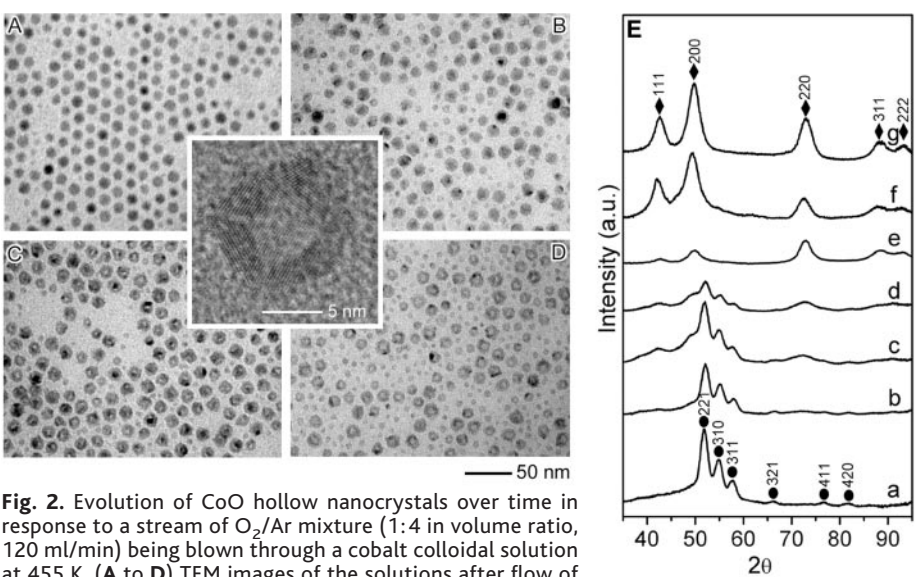

Fig. 2. Evolution of CoO hollow nanocrystals over time in response to a stream of O_2/Ar mixture (1:4 in volume ratio, 120 ml/min) being blown through a cobalt colloidal solution at 455 K. (**A** to **D**) TEM images of the solutions after flow of O_2/Ar for (A) 0 min, (B) 30 min, (C) 80 min, and (D) 210 min. Inset: HRTEM of a CoO hollow nanocrystal. (**E**) XRD patterns of the sample obtained from the solution after flow of O_2/Ar for (a) 0 min, (b) 2.5 min, (c) 5.5 min, (d) 10 min, (e) 30 min, (f) 80 min, and (g) 210 min. The dots and diamonds represent peaks from cobalt and CoO phases, respectively.

at that point, suggesting that small cobalt cores remained. It took ~3 hours for the cobalt cores to be completely consumed; central pores were clearly distinguishable for all nanocrystals under TEM, and the solution showed no magnetic response. XRD simulations (fig. S1) suggest a multicrystalline structure with a crystal domain size of ~3 nm, in agreement with the HRTEM observations (Fig. 2, inset).

The evolution of hollow morphology is best illustrated by following the reaction of cobalt nanocrystals with selenium. In bulk systems, annihilation of excess vacancies at dislocations and boundaries can produce stresses that lead to the formation of cracks near the interface; the cracks then act as nuclei for the further condensation of supersaturated vacancies (*11*). Although the exact mechanism is likely to be different, in nanocrystals voids also begin to develop and merge at the boundary (Fig. 3). The high defect content and surface energy associated with the boundary favor the nucleation of voids there. In addition, as vacancies diffuse inward, they will be more concentrated at the boundary rather than in the interior of the core. As the reaction proceeds in time, more cobalt atoms diffuse out to the shell, and the accompanying transport of vacancies leads to growth and merging of the initial voids. This results in the formation of bridges of material between the core and the shell that persist until the core is completely consumed. These bridges provide a fast transport path for outward diffusion of cobalt atoms that can then spread on the inner shell surface. A similar phenomenon was observed for bulk powders (*11*). The growth rate of pores dropped markedly when the cobalt cores became relatively small. Most of the pore volume seemed to form during the first few minutes, whereas it took ~30 min for the cobalt cores to completely disappear. This may be because, as the bridges are also consumed during the reaction, a smaller cross-sectional area is available for solid-state transport of materials.

As an illustration of the generality of these ideas, we synthesized several other hollow nanostructures. Sulfidation of disk-shaped cobalt nanocrystals (*21*) was observed to result in the formation of hollow nanodisks with cylindrical pores, indicating that spherical symmetry is not required for obtaining shells of regular thickness. Preliminary studies on oxidation of iron nanospheres and sulfidation of cadmium nanospheres also resulted in hollow structures, thus validating our approach for metallic cores in general. Theoretically, the mobilities of the reacting species do not have to be markedly different to result in vacancy transport. Placing solid nanocrystals containing one reactant in a comparatively dilute solution creates an additional asymmetry that may favor the creation of hollow structures: The relatively large change in the concentration of the core material between the core and the solution provides a greater driving force for the outward diffusion of the core material. Thus, numerous combinations of reactants may be expected to produce various hollow nanostructures of insulators, semiconductors, and even metals. A recent report on the formation of gold nanoboxes may involve the same mechanism at some stage, although the dimension of the structures produced is an order of magnitude larger (*22*).

Hollow nanocrystals offer possibilities in material design for applications in catalysis, nanoelectronics, nano-optics, drug delivery systems, and as building blocks for lightweight structural materials (*23*–*25*). For example, accurate fixation of the catalyst within the pores, combined with other emerging techniques of chemical control (*26*), could result in better reaction control and new products. To demonstrate the use of hollow nanocrystals in catalysis, we studied their function as nanoreactors, each of which contains one noble metal nanocrystal. A Pt@CoO yolk-shell nanostructure was synthesized, in which a platinum nanocrystal of a few nanometers was encapsulated in a CoO shell. Three steps were involved in the preparation of these nanoreactors: the synthesis of platinum seeds by a modified "polyol" process (*27*), the deposition of cobalt on platinum to form Pt@Co core-shell nanocrystals, and the transformation of cobalt into CoO hollow structures (*28*). Figure 4A shows a typical sample of platinum particles with an average diameter of ~3 nm. The deposition of cobalt onto platinum at the reaction temperature yielded no alloy, only Pt core/Co shell particles, as confirmed by XRD analyses. The oxidation reaction removed cobalt atoms away from the platinum particle surface, leading to the formation of a platinum yolk/CoO shell structure (Fig. 4B). No free platinum particles were found by TEM inspection of the Pt@CoO sample. We could control the size of Pt@CoO particles by changing the diameter and number of the platinum seeds and the amount of cobalt carbonyl precursor.

In order to determine if the Pt@CoO materials were active as heterogeneous catalysts, we chose the hydrogenation of ethylene as a model reaction, because it readily occurs at ambient conditions on many transition metal catalysts. Platinum is one of the most active metals for this reaction, whereas the activity of metallic cobalt is ~2 orders of magnitude

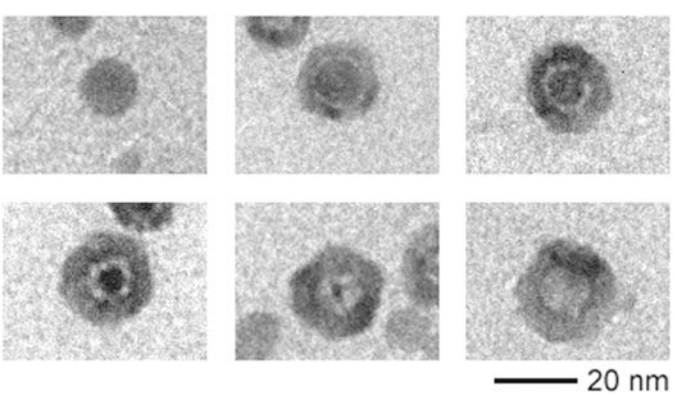

Fig. 3. Evolution of CoSe hollow nanocrystals with time by injection of a suspension of selenium in *o*-dichlorobenzene into a cobalt nanocrystal solution at 455 K, from top-left to bottom-right: 0 s, 10 s, 20 s, 1 min, 2 min, and 30 min. The Co/Se molar ratio was 1:1.

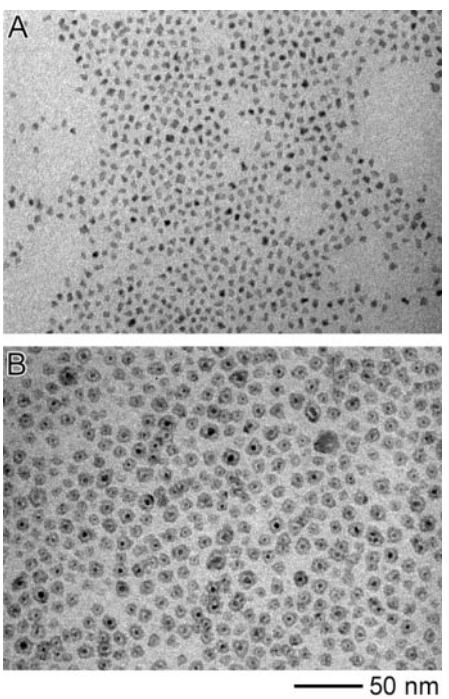

Fig. 4. (**A**) Platinum nanocrystals prepared by the injection of a solution of 0.15 g of platinum acetylacetonate in 5 ml of *o*-dichlorobenzene into a refluxing bath of 10 ml of *o*-dichlorobenzene that contained 0.3 g of 1,2-hexadecanediol, 0.1 ml of oleic acid, 0.1 ml of oleylamine, and 0.06 ml of trioctylphosphine. The solution was then heated for another 120 min. (**B**) We formed Pt@CoO yolk-shell nanostructures by injecting 1.08 g $Co_2(CO)_8$ in 6 ml of *o*-dichlorobenzene into the platinum nanocrystals solution, and followed by the oxidation of the product particles by blowing a stream of O_2/Ar mixture (1:4 in volume ratio, 120 ml/min) into the colloidal solution at 455 K. The system was kept at the same temperature under stirring for 3 hours.

lower (*29*). We found that pure CoO hollow nanocrystals were inactive for ethylene hydrogenation (*30*), even after a 1-hour H_2 prereduction at 373 K. Only on reduction at 473 K for 1 hour was ethane detected at temperatures >300 K. Samples containing platinum without pretreatment were active for C_2H_4 hydrogenation at temperatures as low as 208 K. The steady-state turnover frequency for ethane formation at 227 K was 8.3×10^{-3} s^{-1} (*31*), which is comparable to the rates of 3.5×10^{-2} s^{-1} measured on a 0.04% Pt/SiO_2 catalyst (*32*) and 1.7×10^{-2} s^{-1} measured on pure platinum powders (0.2 to 1.6 μm in diameter). These observations indicate that the reaction is catalyzed by platinum particles, not the CoO shell. This also confirms that a route exists for ethylene and hydrogen entry into the CoO shell interior. The grain boundaries on the shell are the most probable entry points for ethylene and hydrogen diffusion into as well as ethane diffusion out of the shell.

In comparison to catalysts supported on other mesoporous materials, the isolation of catalyst nanoparticles within solid shells should minimize secondary reaction of the products that degrade selectivity and product distribution. Furthermore, any synergistic interactions between catalyst and support can be more efficiently used when each catalyst particle is in contact with a shell of the support material.

References and Notes

1. D. Zhao, P. Yang, Q. Huo, B. F. Chmelka, G. D. Stucky, *Curr. Opin. Solid State Mater. Sci.* **3**, 111 (1998).
2. S. A. Johnson, P. J. Ollivier, T. E. Mallouk, *Science* **283**, 963 (1999).
3. A.-P. Li, F. Müller, A. Birner, K. Nielsch, U. Gösele, *Adv. Mater.* **11**, 483 (1999).
4. D. Trong On, D. Desplantier-Giscard, C. Danumah, S. Kaliaguine, *Appl. Catal.* **222**, 299 (2001).
5. M. E. Davis, *Nature* **417**, 813 (2002).
6. W. Gu, M. Warrier, V. Ramamurthy, R. G. Weiss, *J. Am. Chem. Soc.* **121**, 9467 (1999).
7. A. D. Smigelskas, E. O. Kirkendall, *Trans. AIME* **171**, 130 (1947).
8. C. E. Birchenall, *J. Electrochem. Soc.* **103**, 619 (1956).
9. J. C. Colson, M. Lambertin, P. Barret, in *Proc. 7th Int. Symp. Reactivity of Solids*, J. S. Anderson, F. S. Stone, M. W. Roberts, Eds. (Chapman & Hall, London, 1972), pp. 283–293.
10. G. B. Gibbs, *Oxid. Met.* **16**, 147 (1981).
11. F. Aldinger, *Acta Met.* **22**, 923 (1974).
12. C. B. Murray, C. R. Kagan, M. G. Bawendi, *Annu. Rev. Mater. Sci.* **30**, 545 (2000).
13. X. Peng *et al.*, *Nature* **404**, 59 (2000).
14. R. Jin *et al.*, *Nature* **425**, 487 (2003).
15. V. F. Puntes, K. M. Krishnan, A. P. Alivisatos, *Science* **291**, 2115 (2001).
16. S. Mrowec, K. Przybylski, *Oxid. Met.* **11**, 365 (1977).
17. A. Devin, *Cobalt* **30**, 19 (1966).
18. S. Mrowec, M. Danlelewski, A. Wojtowicz, *J. Mater. Sci.* **33**, 2617 (1998).
19. V. F. Puntes, K. M. Krishnan, P. Alivisatos, *Appl. Phys. Lett.* **78**, 2187 (2001).
20. N. M. Ghoniem, D. Walgraef, S. J. Zinkle, *J. Comput. Aided Mater. Des.* **8**, 1 (2001).
21. V. F. Puntes, D. Zanchet, C. K. Erdonmez, A. P. Alivisatos, *J. Am. Chem. Soc.* **124**, 12874 (2002).
22. Y. Sun, Y. Xia, *Science* **298**, 2176 (2002).
23. F. Caruso, R. A. Caruso, H. Möhwald, *Science* **282**, 1111 (1998).
24. U. S. Schwarz, S. A. Safran, *Phys. Rev. E* **62**, 6957 (2000).
25. W. S. Sanders, L. J. Gibson, *Mater. Sci. Eng. A* **352**, 150 (2003).
26. N. J. Turro, *Acc. Chem. Res.* **33**, 637 (2000).
27. N. S. Sobal, U. Ebels, H. Möhwald, M. Giersig, *J. Phys. Chem.* **107**, 7351 (2003).
28. Platinum acetylacetonate was reduced with a long-chain polyol to form uniform platinum nanoparticles in the presence of surfactants such as oleic acid, oleylamine, and trioctylphosphine. The size of the platinum particles was tuned from 1 to 10 nm, depending on the concentration of surfactants. $Co_2(CO)_8$ was then injected into the hot solution and decomposed to form a conformal coating on platinum nanocrystals. Oxidation of the Pt@Co nanocrystals was performed a few minutes after we introduced the cobalt carbonyl by blowing a stream of O_2/Ar mixture (1:4 in volume ratio, 120 ml/min) into the colloidal solution at 455 K. The system was kept under stirring for 3 hours. A black stable colloidal dispersion in *o*-dichlorobenzene was obtained. Finally, the Pt@CoO particles were precipitated by methanol, washed with toluene and methanol three times, and dried under vacuum. Typical nitrogen adsorption/desorption measurement on the powder at 77 K showed a type IV isotherm with type H2 hysteresis, with a Brunauer-Emmet-Teller surface area of 65 m^2/g and a total pore volume of 0.0676 cm^3/g.
29. G. A. Somorjai, *Introduction to Surface Chemistry and Catalysis* (Wiley, New York, 1994).
30. The hydrogenation of ethylene was studied at atmospheric pressure in a differentially operated plug flow reactor. Standard conditions were 11 Torr of C_2H_4, 150 Torr of H_2, and 208 to 353 K (sample-dependent).
31. Rates were measured on a per-gram basis. They were normalized per mole of surface platinum species (Pt_s) to obtain a turnover frequency (molecule Pt_s^{-1} s^{-1}). Moles of Pt_s was determined by $D = 1.13/d$, where D is the platinum dispersion [the ratio of Pt_s to the total platinum content (Pt_t)] and d is the particle size in nm. The platinum particle size was determined from number average TEM measurements.
32. R. D. Cortright, S. A. Goddard, J. E. Rekoske, J. E. Dumesic, *J. Catal.* **127**, 342 (1991).

33. We thank J. Fréchet for the valuable discussions. Supported by the Air Force Office of Scientific Research under award no. F49620-01-1-0033; by the Director, Office of Energy Research, Office of Science, Division of Materials Sciences, of the U.S. Department of Energy under contract no. DE-AC03-76SF00098; and by the Ford Motor Company and the Berkeley Catalysis Center (R.M.R.).

Supporting Online Material

www.sciencemag.org/cgi/content/full/304/5671/711/DC1
Fig. S1

9 February 2004; accepted 16 March 2004

Population-Level HIV Declines and Behavioral Risk Avoidance in Uganda

Rand L. Stoneburner* and Daniel Low-Beer

Uganda provides the clearest example that human immunodeficiency virus (HIV) is preventable if populations are mobilized to avoid risk. Despite limited resources, Uganda has shown a 70% decline in HIV prevalence since the early 1990s, linked to a 60% reduction in casual sex. The response in Uganda appears to be distinctively associated with communication about acquired immunodeficiency syndrome (AIDS) through social networks. Despite substantial condom use and promotion of biomedical approaches, other African countries have shown neither similar behavioral responses nor HIV prevalence declines of the same scale. The Ugandan success is equivalent to a vaccine of 80% effectiveness. Its replication will require changes in global HIV/AIDS intervention policies and their evaluation.

Projections of the HIV pandemic paint a bleak picture for global health (*1*, *2*). Nevertheless, because most cases of HIV occur through consensual sexual intercourse, it is avoidable if populations are warned and mobilized to change risk-taking behaviors. Despite successes from this approach, the apparently unrelenting expansion of the pandemic has served to emphasize a need for the promotion of more effective responses (*3–5*).

HIV risk behaviors and infection rates dropped substantially among homosexual males in North America and Europe in the early to mid-1980s (*6–8*). The next widely acknowledged success was in heterosexuals in Thailand, a result that has been unequivocally accepted since the early 1990s (*9*). Then, in 1994–1995, came data from resource-poor Uganda of declines in HIV prevalence among younger pregnant women, coupled with indications of preceding behavior change and reductions in HIV incidence (*10–15*). The Ugandan evidence is still viewed with caution, and confusion persists in its evaluation (*16–19*).

We reviewed population-level HIV and behavioral data in Uganda and in neighboring countries to evaluate the validity and determinants of HIV declines and to explore possible influences of preventive interventions (*20*, *21*).

Our initial analysis indicated that HIV incidence was declining in Uganda by the late 1980s (*22–24*). By 1995, Ugandan surveillance of HIV prevalence in pregnant women

Population Health Evaluation Unit, Cambridge University, Cambridge, UK.

*To whom correspondence should be addressed. E-mail: randstoneburner@netzero.net